Check for updates

Wettability of soft PLGA surfaces predicted by experimentally augmented atomistic models

Francesco Maria Bellussi, Otello Maria Roscioni, Edoardo Rossi, Annalisa Cardellini, Marina Provenzano, Luca Persichetti, Valeriya Kudryavtseva, Gleb Sukhorukov, Pietro Asinari, Marco Sebastiani,* and Matteo Fasano* [ID]

A challenging topic in surface engineering is predicting the wetting properties of soft interfaces with different liquids. However, a robust computational protocol suitable for predicting wettability with molecular precision is still lacking. In this article, we propose a workflow based on molecular dynamics simulations to predict the wettability of polymer surfaces and test it against the experimental contact angle of several polar and nonpolar liquids, namely water, formamide, toluene, and hexane. The specific case study addressed here focuses on a poly(lactic-co-glycolic acid) (PLGA) flat surface, but the proposed experimental-modeling protocol may have broader fields of application. The structural properties of PLGA slabs have been modeled on the surface roughness determined with microscopy measurements, while the computed surface tensions and contact angles were validated against standardized characterization tests, reaching a discrepancy of less than 3% in the case of water. Overall, this work represents the initial step toward an integrated multiscale framework for predicting the wettability of more complex soft interfaces, which will eventually take into account the effect of surface topology at higher scales and synergically be employed with experimental characterization techniques.

Impact statement

Controlling the wettability of surfaces has important implications for energy (e.g., self-cleaning solar panels), mechanical (e.g., enhanced heat transfer), chemical (e.g., fluids separation), and biomedical (e.g., implants biocompatibility) industries. Wetting properties arise from a combination of chemical and physical features of surfaces, which are inherently intertwined and multiscale. Therefore, tailoring wettability to target functionalities is a time-intensive process, especially if relying on a trial-and-error approach only. This becomes even more challenging with soft materials, since their surface configuration depends on the solid-liquid interactions at the molecular level and could not be defined *a priori*. The improved accuracy of atomistic models allows detailing how the effective properties of materials arise from their nanoscale features. In this article, we propose and validate a new molecular dynamics protocol for assessing the wettability of soft interfaces with polar and nonpolar liquids. The prediction capabilities of simulations are augmented by a close comparison with microscopy and contact angle experiments. Since smooth copolymer surfaces are considered, here the effort mainly focuses on the effect of chemical features on wettability. In perspective, the proposed atomistic *in silico* approach could be coupled with computational models at higher scales to include the effect of surface microstructures, eventually easing the development of multi-scale surfaces with tunable wettability.

Introduction

The study of soft interfaces is an attractive topic for scientists and engineers due to the broad range of industrial applications dependent on surface properties, such as energy-saving films,[1] antibacterial coatings,[2] biodegradable scaffolding for tissue regeneration,[3,4] rheological and mechanical control,[5,6] phase-separation membranes and interfaces,[7–9] and polymer sensors.[10]

From an experimental standpoint, different techniques have been used to characterize soft surfaces, giving an insight into their chemical, physical, structural, and topological properties. Spectroscopy analysis is commonly used to highlight

Francesco Maria Bellussi, Department of Energy, Politecnico di Torino, Turin, Italy
Otello Maria Roscioni, MaterialX Ltd., Easton Business Centre, Bristol, UK
Edoardo Rossi, Department of Engineering, Università degli studi Roma Tre, Rome, Italy
Annalisa Cardellini, Department of Energy, Politecnico di Torino, Turin, Italy
Marina Provenzano, Department of Energy, Politecnico di Torino, Turin, Italy
Luca Persichetti, Department of Science, Università degli studi Roma Tre, Rome, Iltaly; Department of Physics, Tor Vergata University, Rome, Italy
Valeriya Kudryavtseva, School of Engineering and Materials Science, Queen Mary University of London, London, UK
Gleb Sukhorukov, School of Engineering and Materials Science, Queen Mary University of London, London, UK
Pietro Asinari, Department of Energy, Politecnico di Torino, Turin, Italy; Istituto Nazionale di Ricerca Metrologica, Turin, Italy
Marco Sebastiani, Department of Engineering, Università degli studi Roma Tre, Rome, Iltaly; marco.sebastiani@uniroma3.it
Matteo Fasano, Department of Energy, Politecnico di Torino, Turin, Italy; matteo.fasano@polito.it
*Corresponding author

the molecular composition,[11,12] electronic microscopy,[13] and scanning probe microscopy[14] to analyze the topology, whereas contact angle (CA) measurement[15] to quantify the surface free energy (SFE, using Girifalco or Owens–Wendt models[16,17]). Moreover, recent developments in contact-mechanics-based protocols have been proposed as alternative means to investigate SFE at the microscale via the Johnson–Kendall–Roberts (JKR) or Derjaguin–Muller–Toporov (DMT) models.[18] However, the principal limitation of experimental characterization alone is the lengthy trial-and-error approach, which involves looping over the cycle of materials design, production, and analysis, thus extending the time of prototyping and, consequently, commercialization.[19] In this scenario, computational experiments can help predict the role played by the chemical and topological characteristics on the effective properties of soft interfaces across multiple scales, therefore providing a rational design of their composition and structure according to the required target performance.[20,21] Given the time and space scales involved in wetting phenomena,[22] the adopted computational methods must include a combination of models from the continuum to the atomistic scale.

Since the pioneering study of Young,[23] several continuum models have been proposed to describe the dependence of the static contact angle and dynamical wetting process with surface morphology. Generally, the CA of a liquid on a surface can be correlated to the surface tension components solid/vapor (γ_{sg}), solid/liquid (γ_{sl}), and liquid/vapor (γ_{lg}), through the Young equation:[24]

$$\gamma_{sg} = \gamma_{sl} + \gamma_{lg} \cos \theta_Y, \qquad 1$$

where θ_Y is the Young CA, which depends only on the chemistry of the liquid and solid phases. Despite its simplicity, this relation is valid only for ideal flat surfaces. The CA obtained experimentally corresponds to the apparent CA, which depends also on the surface roughness and morphology. According to the Wenzel and Cassie–Baxter models of static contact angle on rough surfaces,[24–26] the Young or local contact angle can be included in continuum models as a boundary condition on the wetted wall. This value depends on the surface chemistry of the material, and it can be provided by experiments performed on a perfectly flat surface or—as highlighted in the work of Johansson et al.[27,28]—by molecular dynamics (MD) simulations.

At the atomistic level, an increasing number of studies have focused on wettability. Leroy et al. used the free energy perturbation approach (FEP)[29,30] to evaluate the CA of water on graphene and, consequently, to calibrate their interaction parameters. Similarly, Zhang et al.[31] employed the FEP to parametrize the interaction of water with fresh and aged molybdenum disulfide (MoS_2) surfaces, whereas Rajan et al.[32] used the FEP and the Green–Kubo relation to evaluate the work of adhesion and friction coefficient of water and other solvents on a hexagonal boron nitride surface. In our previous work,[33] we highlighted that a synergistic use of MD simulations and experiments allows discriminating how surface chemistry and topology

of a hydrophobic coating contribute to increasing the contact angle of water. The CA assessment by MD can be carried out also via the droplet method, where a liquid drop is positioned above the tested surface and then left to relax until equilibrium conditions are reached. Using this method, Yaghoubi et al. and Koishi et al.[34–36] studied the effect of roughness on the wettability of graphite surfaces, whereas Sresht et al. assessed MoS_2 surfaces.[37] In such simulations, the solid substrate is typically modeled as a rigid crystal, thus neglecting deformation effects at the solid–liquid interface. Similarly, Liu et al.,[38] Zhu et al.,[39] and Etha et al.[40] applied the droplet method to soft surfaces, keeping the substrate rigid to preserve the planar configuration of the interface. However, in the case of soft surfaces such as for polymers, the interfacial deformation of the solid substrate and its effect on wettability cannot be neglected to accurately reproduce the actual experimental conditions. Hence, the characteristic deformable boundary of soft interfaces requires new (and validated) 3D simulations and post-processing protocols for the CA measurement by MD, especially for the definition of the mean plane where the contact angle is evaluated.

In this work, we propose and validate a new MD protocol, based on the sessile droplet method, for assessing the wettability of smooth, soft interfaces with polar and nonpolar liquids. In detail, we:

1. Validate the force field by computing the density and glass-transition temperature of a soft material (a polymer), the density and surface tension of the probe liquids, and comparing the computed values with the experimental data available.
2. Create a MD sample whose surface matches the experimental topology of the soft material.
3. Simulate the 3D sessile droplet experiment by evaluating the apparent contact angle from the MD trajectory.

The proposed protocol is employed to study the wettability of poly(lactic-*co*-glycolic acid) (PLGA) surfaces with water, formamide, toluene, and hexane (**Figure 1**). PLGA is a copolymer formed by repeating units of lactic acid (LA) and glycolic acid (GA). PLGA is a relevant case study because its wetting properties determine its biocompatibility and biodegradability in many biomedical applications.[41–43] In perspective, this validated protocol can be easily transferred to study flat and rough surfaces of both soft and hard materials, with a promising synergistic potential with respect to experimental characterization techniques.

Results and discussion

The characterization protocol discussed in this work employs MD simulations to predict the wetting properties of soft interfaces. The details related to the model building process are reported in the "Materials and methods" section.

The wetting properties of PLGA surfaces are assessed after carefully evaluating the bulk properties of the polymer slab and the probe liquids. First, we evaluate the density
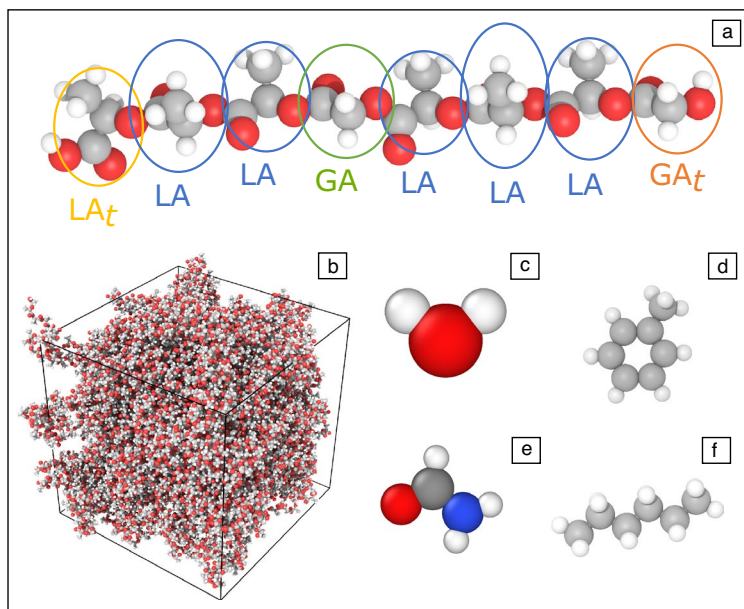
Figure 1. Materials considered in the molecular dynamics simulations. (a) Oligomer of PLGA with the lactic (LA and LA$_t$) and glycolic (GA and GA$_t$) monomers highlighted. The subscript t indicates the terminal residuals. (b) Condensed sample of bulk PLGA (box dimension 73 Å). This equilibrated PLGA box was then replicated three times in the x and y directions to create a supercell for the contact angle modeling measurements. (c) Water (SPC-E, Tip4P-05), (d) toluene, (e) formamide, and (f) hexane molecules used in the simulations. Elements are represented by different colors: carbon in gray, oxygen in red, hydrogen in white, and nitrogen in blue.

and glass-transition temperature (T_g) of the simulated PLGA bulk. The density of PLGA computed at 300 K during the equilibrated MD trajectory is equal to 1.275 ± 0.025 g/cm^3, in excellent agreement with the experimental value (1.30

g/cm^3)[44]. The T_g was evaluated by performing a scan in temperature and monitoring the variation of density.[45] In **Figure 2**a, we report the density of PLGA against temperature, identifying the two distinct branches of the plastic and glassy states. These branches are interpolated with two linear regressions, intercepting at a temperature $T_g = 328$ K that accurately matches the experimental value of 320–330 K.[44]

Similarly, we evaluate the density of the probe liquids at 300 K and 1 atm, finding an excellent agreement with the experimental evidence from the literature (see Table SI in the Supplementary information). For the specific case of water in contact with the polymer substrate, we investigate the coupling of the two phases by considering a liquid film onto the polymer slab and evaluating the density profile along the normal direction to the polymer surface.[46] Results in Figure 2b show an overlap between the two phases in the contact region due to the soft (polymer/water) interface, while the nominal densities of PLGA and pure water are eventually recovered after the interface. In **Figure 5**a, we report the calculated surface tension for the four liquids, finding that MD results are in good agreement with both experimental and other numerical results available in the literature[47–51] (see Table SI in the Supplementary information for details). This evidence supports the reliability of the force field used to describe the PLGA and probe solvents, thus providing confidence for predicting the wetting properties of surfaces.
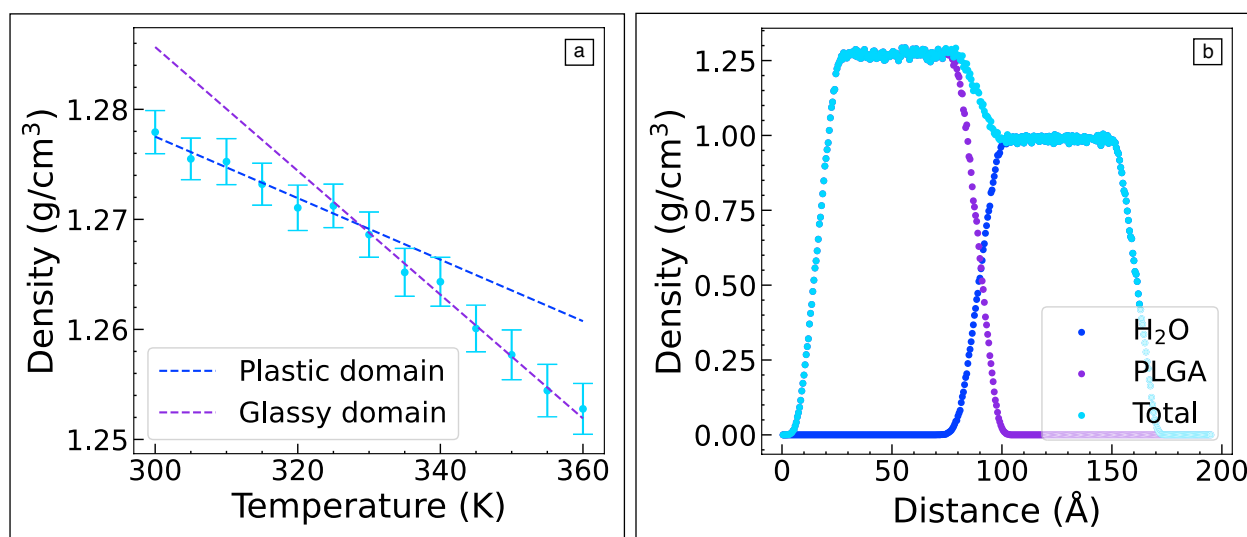

Figure 2. (a) Evaluation of the glass-transition temperature of the simulated PLGA sample, obtained from the interpolation of the plastic (in blue) and glassy (in violet) branches. (b) Simulated density profile at the water/PLGA interface, measured on a water film approximately 70 Å thick onto the polymer slab.

Second, we characterize the topography of the PLGA surface in terms of the root-mean-square (rms) roughness of the MD sample, comparing this value with that obtained by atomic force microscopy (AFM) measurements. The smallest viable experimental scans are of 100 nm × 100 nm, from which representative zoomed sections were extracted with a lateral dimension comparable to that of the MD samples (see **Figure 3**). The rms roughness of the numerical and experimental samples is 3.2 Å and 2.2 Å, respectively. According to the Wenzel model for hydrophilic surfaces[25,52,53] (i.e., $\cos\theta = R_f \cos\theta_Y$, where θ is the apparent CA, θ_Y the Young CA, and $R_f = \frac{A_{eff}}{A_{proj}}$ the roughness factor, being A_{eff} the effective area of the polymer surface and A_{proj} the projected area on the acquisition window), we found the experimental roughness factor in the range of 1.0570–1.1078 depending on the scan size (see Table SII in the Supplementary information) and 1.5250 in the MD sample. Considering the non-periodicity of the PLGA surface features (as analyzed from 2D fast Fourier transform of AFM scans), the influence of surface topology on the measured CA is smaller than 5% for the conducted experimental tests, thus within the statistical uncertainty of the measure. Consequently, the CA obtained from experiments and simulations can be considered as the Young CA with good approximation ($\theta \approx \theta_Y$). The only notable exception is the case of formamide on PLGA, where the low value of θ leads to larger deviations from θ_Y (see Table SII in the Supplementary information).

Third, the CA of the four liquids on the flat PLGA surface are computed and compared against the experimental measurements. In the case of water droplets, the CA of the SPC-E and the Tip4P-05 models was found to be 61.7° ± 3.8° and 64.6° ± 5.0°, respectively, in excellent agreement with the experimental measure of 65° ± 4° (see Figure S1 in the Supplementary information) and previous works from the literature.[54] The hydrophilic nature of the PLGA sample is also highlighted considering the surface free energy of 43 ± 3 mJ/m² evaluated through the Owen–Wendt method[16] (see Note 1 in the Supplementary information). The evolution of a water droplet onto the PLGA surface is shown in **Figure 4a**, where equilibrium conditions are reached after some 500 ps of simulation. The CA is measured during the last 2 ns of trajectory, where the CA oscillates around a stable mean value (see Figure 4b, Tip4P-05 model). The error on the CA is computed by propagating the error on each snapshot due to different choices of δ (see the "Materials and methods" section). As reported in Figure S2 of the Supplementary information, the average CA obtained with the SPC-E water model and the standard deviation of each snapshot is similar to the Tip4P-05 model, proving the reliability of our numerical protocol regardless of the chosen water model. In the case of formamide, we observe a mismatch between the computed (27.3° ± 5.5°) and experimental (52° ± 4°, see Figure S3 in the Supplementary information) CA. Considering the Wenzel model, however, the measured apparent CA (27.3°) can be used to extract the Young CA (54.3°), which results in excellent agreement with the experimental value of θ_Y (see Table SII in the Supplementary information). Furthermore, given the good solubility of formamide in water, we can assume that atmospheric moisture in the testing environment could be absorbed in the formamide droplet during the experimental measurements. However, the perfectly anhydrous conditions in MD simulations can partially also explain the mismatch between numerical and experimental values of CA for formamide. We tested this hypothesis by performing additional simulations with droplets of formamide containing 10% wt and 20% wt of water, using the same computational procedure (see Figure S4–S6 in the Supplementary information). In the first case, we did not observe a significant variation in the evaluated CA, whereas in the second one, the CA reached its equilibrium at a higher CA value, namely 32° ± 9°.

In the case of nonpolar hydrocarbon liquids, the simulations reproduce the high affinity with the PLGA surface observed experimentally with good accuracy. For toluene, MD shows an initial metastable state of the droplet with a CA of 11° ± 2° for approximately 500 ps before a complete spreading is eventually achieved (see Figure S7 in the Supplementary information). During experiments, we observe
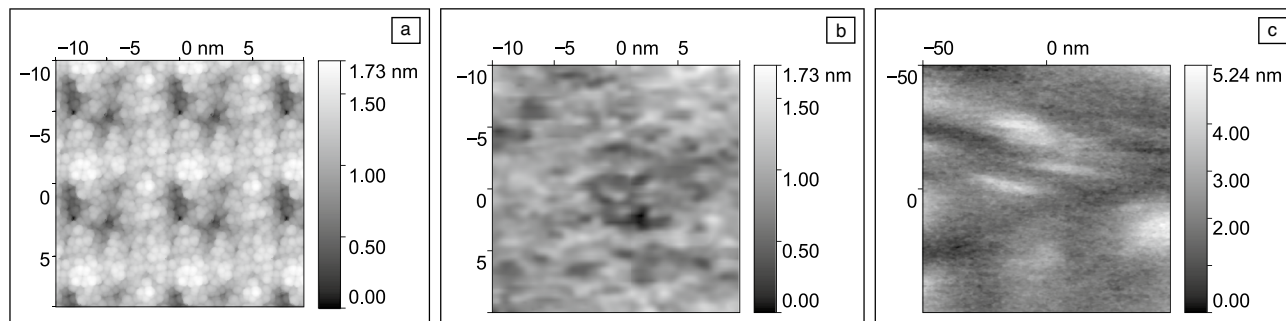
Figure 3. (a) Surface topography analysis of the PLGA sample considered for the molecular dynamics simulations, obtained from a 3×3 super-cell. (b) Experimental topography analysis of the PLGA specimen from atomic force microscopy: representative 20 nm × 20 nm area extracted from the original (c) 100 nm × 100 nm scan.
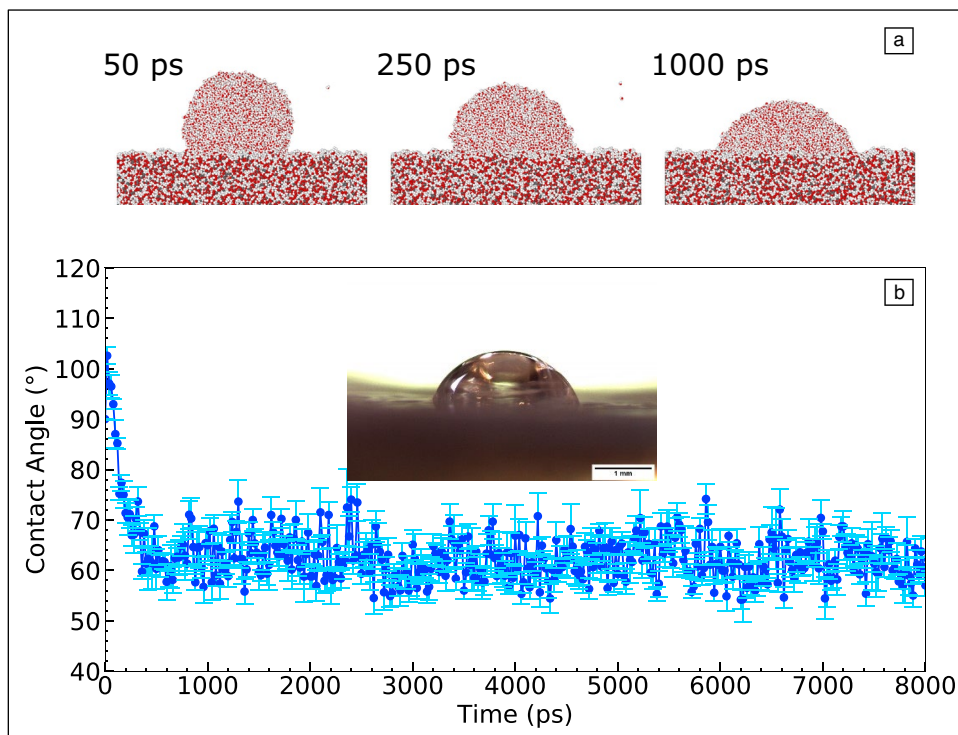
Figure 4. (a) Pictorial view of the Tip4P-05 water droplet evolution during the simulated stabilization on the PLGA surface. (b) Variation of the apparent contact angle (CA) during the stabilization and acquisition trajectory. Data acquired over the last 2 ns. The error bars on CA values come from averaging over different values of δ. The inset in (b) is the water droplet on the flat PLGA sample from which the experimental CA is evaluated.

course, the size of the droplet, whose diameter should not exceed half the periodic box vectors. An elegant way of increasing the size of the droplets while keeping the computational cost at a manageable level is by adopting a pseudo-2D model, where the droplet is replaced by a periodic cylinder.[27,28]
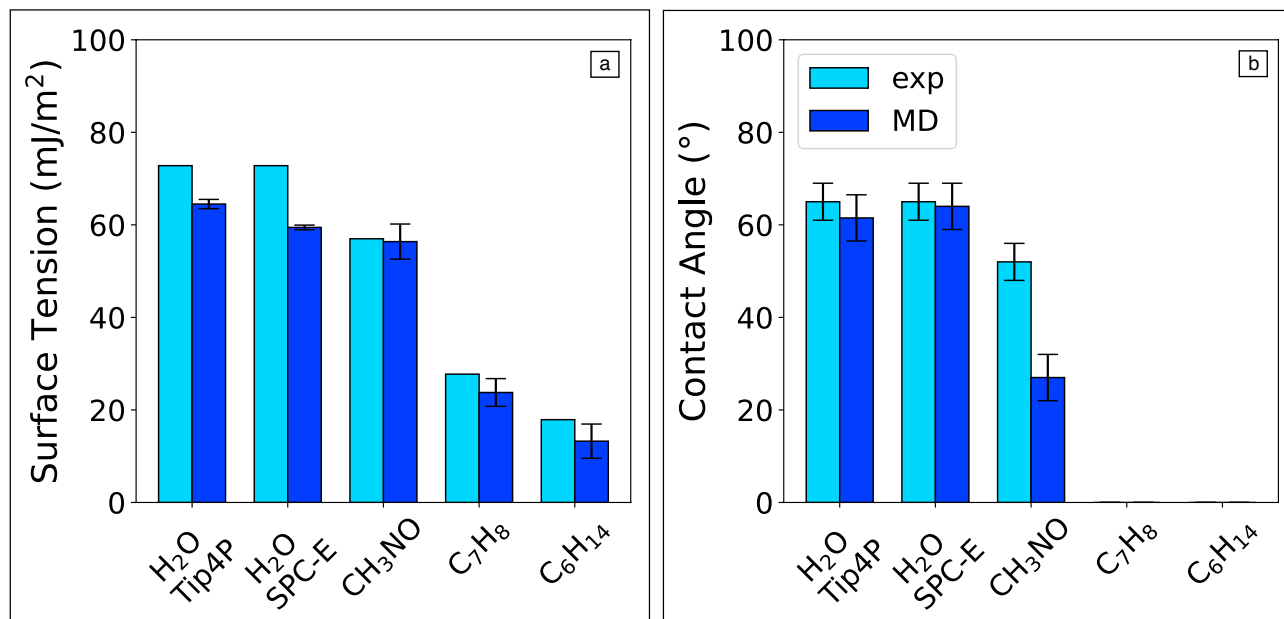
Another significant limitation is the time scale accessible through MD simulations, here on the order of 10 ns per sample. With the parameters used in our MD simulations, most samples reach thermodynamic equilibrium within a few nanoseconds unless other phenomena with more long time scales are involved.[56–58] Although it cannot be ruled out that the observed droplets were in a metastable state lasting longer than the simulated time, we have verified that the contact angle reaches a consistent equilibrium value for droplets of increasing size. In this work, we have used droplets containing approximately 13,000 molecules to limit finite-size effects and reduce the numerical noise of simulations.

A way to overcome the limitations of atomistic models is to decrease the resolution of the system and its internal degrees of freedom, a process known as coarse-graining. A recently developed coarse-grained model, which reproduces the morphology and density of organic semiconductors[59] and polymers,[60] and the structural and dynamic properties of water[61] in quantitative agreement with atomistic MD simulations, will be used in a follow-up study to predict the wetting behavior of soft interfaces, addressing the known limitations of atomistic models but without compromising on the quality of the predicted properties.

This considered, the evaluation of water droplet size-dependent behavior on hydrophilic surfaces from literature data[62] reported that a remarkable effect of surface asperities, within the microstate pinning behavior, is such that a narrowing of contact angle evaluated error from MD simulations occurs for a nanoscale roughened surface. This is in accordance with authors' preliminary evaluations for specific selection of the simulated sessile droplet volume (while roughness itself determines an increase in the CA mean value). As, however, accordance with experimental data are stated throughout this work, it is worth highlighting that our modeling activities reached the pinning state equilibrium.

a stable contact angle of 23° ± 5° for approximately 15 s before a complete spreading (see Figure S8 in the Supplementary information). Indeed, it is worth noting that toluene is a good solvent of PLGA and that the size of the MD sample is orders of magnitude smaller than the experimental one. Hence a shorter time scale is expected for the interaction between the two phases. In the case of hexane, we observe a complete spreading of the droplet onto the PLGA surface (0°; see Figure S9 in the Supplementary information) after approximately 1.2 ns, yielding to formation of a uniform film. This behavior is confirmed experimentally, where an instantaneous spreading of the hexane droplet is observed. The overall comparison between the computed and experimental CA for the four fluids on PLGA is shown in Figure 5b.

The main advantage of the numerical method proposed and validated here is to simplify and accelerate the initial stages of material surface design and prototyping, offering an integrated framework that allows predicting the wettability of a wide range of soft interfaces with good accuracy. However, MD simulations can suffer from artefacts due to finite-size effects.[55] The size of the samples investigated in this work was capped at approximately 350,000 atoms to match the computational resources available. These constraints limit the size of the surface investigated, the maximum roughness that can be realistically modeled on a periodic surface, and of

Figure 5. Comparison between experimental and numerical wetting properties of the PLGA and probe fluids. (a) Surface tension of the probe fluids and (b) their apparent contact angles (CAs) on PLGA. The experimental values of surface tension are taken from References 47–51, whereas those of CAs from measurements carried out in this work. The surface tension from numerical simulations was averaged over 5 ns of acquisition time. The experimental CA was averaged on at least six different droplets for each liquid, whereas the CA from numerical simulations was averaged over 2 ns and different values of δ.

With this goal in mind, this work represents the first step toward the creation of a multiscale model able to predict and optimize the wettability of microstructured soft surfaces, for instance, by providing fast and accurate values of the local or Young contact angle, which in turn can be used as a boundary condition in multiphase continuum models (e.g., finite-elements or finite-volume simulations).

Conclusions
In this work, we reproduced sessile droplet experiments with molecular dynamics simulations, proposing a methodological procedure for predicting the wettability of soft interfaces. In detail, we studied PLGA surfaces wetted by polar and non-polar solvents (water, formamide, toluene, and hexane) and validated the obtained results with experiments.

We initially evaluated the surface topography of the MD and experimental samples through the solvent accessible surface and AFM, respectively. Both numerical and experimental surfaces present a rms roughness smaller than 10 Å, while the roughness factor (R_f) is between 1.0570 and 1.1078 in the experimental samples and 1.5250 in the MD sample. According to the Wenzel theory, the local or Young contact angle can be assessed with droplet experiments under these conditions since negligible effects from surface topology are expected. For the numerical model, the surface topology may affect the measurement of liquids that present a low apparent contact angle, such as formamide. The glass-transition temperature of bulk PLGA and the surface tension of the probe liquids

computed from MD simulations were found to be in excellent agreement with the experimental evidence, thus validating the force field chosen to describe the materials in this study. Finally, we performed the sessile droplet experiment, leaving a droplet of solvent to relax onto the PLGA surface and then measuring the apparent contact angle by post-processing the MD trajectory. The results obtained agree with the experimental measures, therefore supporting the proposed protocol. In the case of water droplets, both the SPC-E and the Tip4P-05 models show an excellent agreement with experiments. With the formamide model, we observe a reduction of approximately 30% with respect to the experimental CA: we attributed this mismatch to the effects of the roughness factor (R_f) according to the Wenzel theory and to the perfectly anhydrous conditions in the MD simulations of formamide droplets, differently from the testing environment. The MD simulations predict a strong affinity of nonpolar solvents with the polymer surface, which was confirmed by the experimental measurements. Toluene spreads over the PLGA surface after a transient metastable state, whereas the hexane droplet spreads immediately.

This work is a relevant case study of convergence and synergy between digital and experimental measurements toward a new class of hybrid characterization standards (e.g., coupled MODA[63] and CHADA[64] workflows). In perspective, the proposed methodology will speed up the development of soft material interfaces with controllable wetting properties. The protocol presented in this work has been shown to accurately predict

the CA of polar and nonpolar solvents on a soft polymeric surface. This information can be used as a boundary condition in continuum simulations able to assess the effect on wettability produced by modifications of the surface topology at the nano- and microscales, thus connecting the property of materials at the device level with their underlying molecular structure.

Materials and methods

Model building

The experimental length of PLGA chains typically comprises between 240 and 390 repeating units, a size that is computationally inaccessible for practical applications based on atomistic simulations. Literature works on PLGA have reported MD simulations with a polymer length between 10 and 90 monomers.[65–68] In this work, we used PLGA chains composed of 48 monomers, corresponding to 12 repetitions of 3 LA monomers and 1 of GA monomer, thus keeping the 75:25 LA to GA ratio of the experimental samples.

The structure of a single PLGA chain was built with Avogadro,[69,70] whereas the condensed PLGA phase was generated starting from a randomly sparse configuration of chains in a simulation box with periodic boundary conditions in the three orthogonal directions (see Figure 1a–b). An initial guess composed of 90 polymer chains in a cubic box with side of 900 Å was created with Moltemplate,[71] whereas the MD simulations were carried out with LAMMPS.[72,73] The OPLS-AA force field[74] was used to describe the interaction potentials of PLGA. The wettability of PLGA was evaluated with four liquids: water (both Tip4P-05[75] and SPC-E[76] models), formamide, toluene, and hexane, which were modeled with the OPLS-AA force field (Figure 1c–f). A cutoff of 1.3 nm was used for nonbonded interactions, with cross-term Lennard-Jones parameters computed with geometric mixing rules. Long-range interactions were computed with the PPPM method with 10^{-4} accuracy.

The equilibration of PLGA samples began with a controlled multistep compression at 1 K, in which the volume of the simulation box was progressively reduced by 15% in each step for 49 steps. The electrostatic interactions were switched off during this process to emulate the screening induced by a virtual solvent. Then, the bulk sample was relaxed in the isobaric-isothermal ensemble (NPT) at 300 K and 1 atm for 2 ns, with nominal electrostatic interactions. Surfaces of PLGA were created by removing the periodic boundary in the z-direction, turning the bulk into a slab geometry. The system was then equilibrated in the canonical ensemble (NVT) at 300 K to allow surface reconstruction for approximately 4 ns. A correction term for systems with slab geometry was added to the long-range electrostatic interactions.[77] The equilibrated surface was then replicated three times in the x and y directions, yielding a square surface with lateral dimension* of

---

* The lateral size of the supercell is approximately two orders of magnitude bigger than the experimental surface roughness.

approximately 220 Å. This supercell was used for CA simulations, as its larger size helped to avoid finite-size effects, which could affect the wetting properties of the soft interface.[34,35]

The topological characterization of PLGA surfaces is based on the solvent accessible surface (SAS) of the slab, computed with the program Jmol[78] on the final configuration of the NVT simulation. The resulting SAS was exported as a triangular mesh and edited with Meshlab[79] to remove the boundary walls. Then, the surface roughness of PLGA was computed with Gwyddion,[80] taking the meshed SAS as input, and compared with the experimentally determined one.

The density and surface tension of the four liquids were used to gauge the accuracy of the force field, by comparing the computed values with the experimental ones. The density was measured on samples made of 1000 molecules in a periodic box reproducing bulk conditions. Each sample was equilibrated in the NPT ensemble at 300 K and 1 atm for 2 ns with coupling constants of 0.1 and 1 ps for temperature and pressure, respectively. The surface tension was calculated on a slab geometry according to the Kirkwood–Buff relation:[81]

$$\gamma_l = \frac{L_z}{2} \left[\langle P_z \rangle - \frac{\langle P_x \rangle + \langle P_y \rangle}{2} \right], \qquad 2$$

where P_z is the liquid pressure in the direction orthogonal to the surface, P_x and P_y are the pressures in the transverse directions, and L_z is the length of the simulation box in the orthogonal direction to the surface, whereas brackets indicate an NVT ensemble average. A production run of 5 ns was used for data acquisition after the slab was equilibrated for 5 ns.

The apparent contact angle of the different liquids on the PLGA slab was computed with numerical experiments following the droplet method. The initial guess of each droplet was a cube of equilibrated liquid with box edges of approximately 73 Å (see **Figure 6**a). The droplet was equilibrated on top of the PLGA slab until the potential energy and the evaluated CA reached a stable value with time. The total number of atoms of the slab/solvent systems was approximately 350'000.

The contact angle was calculated from the MD trajectory using a post-processing code developed for this purpose. We initially define a mean plane representative of the interface, comparing the positions of liquid and polymer surface atoms. The droplet axis was identified from the average position of all the droplet atoms, and the droplet height h from the interface plane. Then, we consider two contiguous liquid slabs (s_1 and s_2) of height δ at a distance δ from the interface plane. We evaluate the radial density profile of the liquid in s_1 and s_2 to estimate the droplet radius r_1 (at z_1, that is the mean z coordinate of s_1) and r_2 (at z_2, that is the mean z coordinate of s_2) in the $x - y$ plane. We measure the radius at the liquid-air interface, defined as the point where the density falls in a range below 50% of the bulk value (see the code available at Reference 82 for details). Finally, the CA is evaluated as $\theta = \arctan(\Delta z / \Delta r)$, where $\Delta r = r_1 - r_2$ and $\Delta z = z_2 - z_1$ (see Figure 6b). This procedure is subject to the choice of δ for the evaluation of r_1 and r_2. Then,
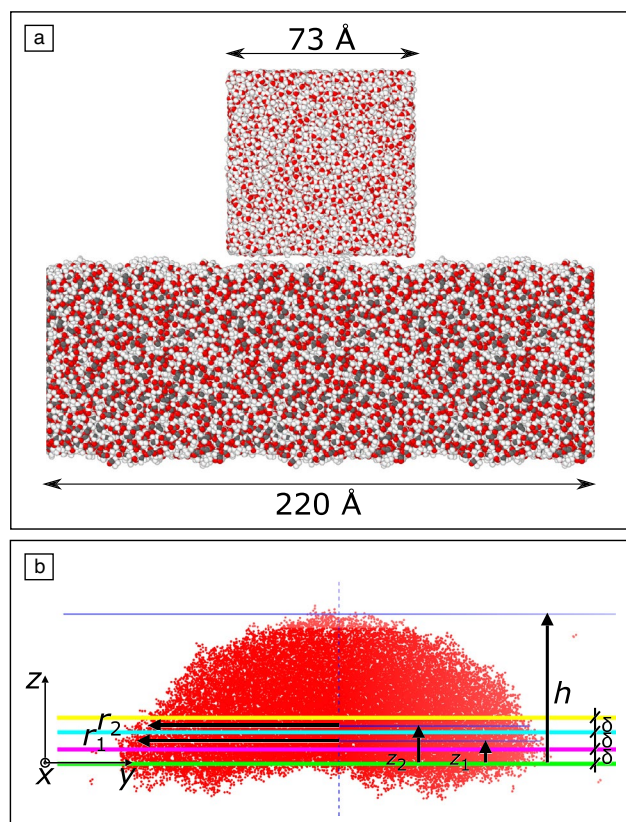
Figure 6. (a) Snapshot of the initial configuration of a water/PLGA sample for molecular dynamics (MD) simulations, detailing the domain size. (b) Schematic view of the process for evaluating the contact angle from the MD trajectory. The dashed blue vertical line identifies the droplet axis; the blue horizontal line the droplet height limit (h); the green line the mean plane between the liquid and soft surface. The liquid slabs s_1 and s_2 are defined between the magenta and cyan lines, and the cyan and the yellow lines, respectively. δ indicates the thickness of s_1 and s_2, whereas z_1 and z_2 the mean line of s_1 and s_2, respectively.

we replicate the procedure with different values of δ, expressed as a percentage of the drop height (within 7% and 10%), and average the CA final value from these results.

Sample preparation

Typical commercial proportions of LA:GA in PLGA samples range from 50:50 to 85:15, 50:50 and 75:25 being the most common ones.[44] The presence of CH_3 side groups makes LA more hydrophobic than GA. Therefore, a copolymer with higher LA content absorbs less water and then degrades more slowly, the 50:50 ratio being the one showing the fastest degradation rate.[41,83]

In this work, we focus on 75:25 copolymers (i.e., 66'000–107'000 g/mol molecular weight) to achieve a good balance between durability and hydrophilicity. The PLGA solution was prepared in a mixture of chloroform (Fisher Chemical, USA) with a concentration of 5% in weight. The solution rested for a homogenization time of 12 h. Then, 2 ml

of solution was poured into a dry petri dish with a diameter of 12 cm, and finally dried until the solvent was fully evaporated and the flat slab of PLGA obtained.

Experimental characterization

The topological characterization of the PLGA samples was performed in terms of the surface root mean square roughness, evaluated using a Bruker atomic force microscope (AFM dimension icon, Bruker) operating in standard tapping mode at a scan rate of 0.996 Hz. The AFM is equipped with a TESP-SS Bruker silicon probe featuring a nominal cantilever elastic constant of 42 N/m and a tip with a nominal radius of 2 nm. The selection of the AFM operating mode and tip radius value is based and cross-validated considering the relative errors (from the true value of rms roughness theoretically approachable using an infinitely sharp tip) arising from eventual convolution effects on surface topography, as elucidated by Sedin et al.[84] Indeed, for small lateral scans (≤500 nm), the image root mean square roughness decreases as tip size increases: in the case of the investigations performed, it has been evaluated an error for a tip radius of 2 nm lesser than 3%, eventually falling within the experimental error associated with surface morphology repeatability. Each measurement was performed on a scan area of 100 nm × 100 nm or 500 nm × 500 nm, where two sensor images were recorded simultaneously (corresponding to forward and backward scans). Images were then analyzed and processed with the software Gwyddion.[80]

The solid–liquid interaction between PLGA and the different fluids was validated by sessile droplet contact angle measurements, employing normative-compliant equipment (UNI EN 828, UNI 9752, ASTM D-5725-99). CA testing was conducted at room temperature (20°C) and relative humidity between 40% and 50 percent. A minimum of six droplets (with a volume of 3 μL each) of water, formamide (polar solvents), toluene, or hexane (nonpolar hydrocarbons) were deposited on the sample surface to measure the apparent contact angle and then estimate the overall surface free energy (SFE) of the PLGA samples. After 60 s of stabilization, images of the liquid drops were captured (LAS-EZ software, Leica Camera AG) and subsequently elaborated (ImageJ software) using a spherical approximation of the droplet shape. This method allows assessing the angle formed between the two tangents of the fitted sphere with the straight line corresponding to the sample surface, thus obtaining the CA value (θ).

Data availability

All data generated or analyzed during this study are included in this published article as supporting information files. All simulation files and post-processing codes are available at the Zenodo archive associated with this work (https://doi.org/10.5281/zenodo.6629427).

Conflict of interest

On behalf of all authors, the corresponding authors state that there is no conflict of interest.

Open access

Supplementary information

The online version contains supplementary material available at https://doi.org/10.1557/s43577-022-00380-9.

References

1. Y. Gao, W. Yao, J. Sun, H. Zhang, Z. Wang, L. Wang, D. Yang, L. Zhang, H. Yang, *J. Mater. Chem. A* **3**, 10738 (2015). https://doi.org/10.1039/C4TA06347C
2. N. Cottenye, K. Anselme, L. Ploux, C. Vebert-Nardin, *Adv. Funct. Mater.* **22**(23), 4891 (2012). https://doi.org/10.1002/adfm.201200988
3. S.S. Liow, A.A. Karim, X.J. Loh, *MRS Bull.* **41**(7), 557 (2016). https://doi.org/10.1557/mrs.2016.139
4. A. Cardellini, M. Fasano, E. Chiavazzo, P. Asinari, *Phys. Lett. A* **380**(20), 1735 (2016). https://doi.org/10.1016/j.physleta.2016.03.015
5. Q. Chen, X. Zhang, K. Chen, X. Wu, T. Zong, C. Feng, D. Zhang, *Chem. Eng. J.* **430**, 133036 (2022). https://doi.org/10.1016/j.cej.2021.133036
6. J.E. Mates, R. Ibrahim, A. Vera, S. Guggenheim, J. Qin, D. Calewarts, D.E. Waldroup, C.M. Megaridis, *Green Chem.* **18**(7), 2185 (2016). https://doi.org/10.1039/C5GC02725J
7. D. Ballal, W.G. Chapman, *J. Chem. Phys.* **139**(11), 114706 (2013). https://doi.org/10.1063/1.4821604
8. H.-C. Yang, Y. Xie, H. Chan, B. Narayanan, L. Chen, R.Z. Waldman, S.K. Sankaranarayanan, J.W. Elam, S.B. Darling, *ACS Nano* **12**(8), 8678 (2018). https://doi.org/10.1021/acsnano.8b04632
9. M. Fasano, A. Bevilacqua, E. Chiavazzo, T. Humplik, P. Asinari, *Sci. Rep.* **9**(1), 1 (2019). https://doi.org/10.1038/s41598-019-54751-5
10. P. Wang, G. Zheng, K. Dai, C. Liu, C. Shen, *Chem. Eng. J.* **430**, 133052 (2022). https://doi.org/10.1016/j.cej.2021.133052
11. R. Mažeikienė, G. Niaura, A. Malinauskas, *Spectrochim. Acta A Mol. Biomol. Spectrosc.* **262**, 120140 (2021). https://doi.org/10.1016/j.saa.2021.120140
12. T.T. Nguyen, H.T.T. Khuat, S. Asakura, G. Mizutani, Y. Murakami, T. Okada, *J. Chem. Phys.* **155**(8), 084702 (2021). https://doi.org/10.1063/5.0057145
13. W. Wang, H. Li, Q. Li, Z. Luo, *J. Appl. Polym. Sci.* **138**(42), 51242 (2021). https://doi.org/10.1002/app.51242
14. J. Delabie, J. De Winter, O. Deschaume, C. Bartic, P. Gerbaux, T. Verbiest, G. Koeckelberghs, *Macromolecules* **53**(24), 11098 (2020). https://doi.org/10.1021/acs.macromol.0c01593
15. J. Gerber, T. Lendenmann, H. Eghlidi, T.M. Schutzius, D. Poulikakos, *Nat. Commun.* **10**(1), 4776 (2019). https://doi.org/10.1038/s41467-019-12093-w
16. D.K. Owens, R.C. Wendt, *J. Appl. Polym. Sci.* **13**(8), 1741 (1969). https://doi.org/10.1002/app.1969.070130815
17. R.J. Good, L.A. Girifalco, *J. Phys. Chem.* **64**(5), 561 (1960). https://doi.org/10.1021/j100834a012
18. E.M. Rossi, P.S. Phani, R. Guillemet, J. Cholet, D. Jussey, W.C. Oliver, M. Sebastiani, *J. Mater. Res.* **36**(11), 2357 (2021). https://doi.org/10.1557/s43578-021-00127-3
19. B.S. Guiton, M. Stefik, V. Augustyn, S. Banerjee, C.J. Bardeen, B.M. Bartlett, J. Li, V. López-Mejías, L.R. MacGillivray, A. Morris, E.E. Rodriguez, A.C.S. Samia, H. Sun, P. Sutter, D.R. Talham, *MRS Bull.* **45**(11), 951 (2020). https://doi.org/10.1557/mrs.2020.271
20. T.-S. Wong, T. Sun, L. Feng, J. Aizenberg, *MRS Bull.* **38**(5), 366 (2013). https://doi.org/10.1557/mrs.2013.99
21. M.J. Buehler, *MRS Bull.* **38**(2), 169 (2013). https://doi.org/10.1557/mrs.2013.26
22. D. Bonn, J. Eggers, J. Indekeu, J. Meunier, E. Rolley, *Rev. Mod. Phys.* **81**, 739 (2009). https://doi.org/10.1103/RevModPhys.81.739
23. T. Young III, *Philos. Trans. R. Soc. Lond.* **95**, 65 (1805). https://doi.org/10.1098/rstl.1805.0005
24. E. Bormashenko, *J. Colloid Interface Sci.* **360**(1), 317 (2011). https://doi.org/10.1016/j.jcis.2011.04.051
25. R.N. Wenzel, *Ind. Eng. Chem.* **28**(8), 988 (1936). https://doi.org/10.1021/ie50320a024
26. A.B.D. Cassie, S. Baxter, *Trans. Faraday Soc.* **40**, 546 (1944). https://doi.org/10.1039/TF9444000546
27. P. Johansson, B. Hess, *Phys. Rev. Fluids* **3**, 074201 (2018). https://doi.org/10.1103/PhysRevFluids.3.074201
28. P. Johansson, A. Carlson, B. Hess, *J. Fluid Mech.* **781**, 695 (2015). https://doi.org/10.1017/jfm.2015.517
29. F. Leroy, F. Müller-Plathe, *Langmuir* **31**(30), 8335 (2015). https://doi.org/10.1021/acs.langmuir.5b01394
30. F. Leroy, S. Liu, J. Zhang, *J. Phys. Chem. C* **119**(51), 28470 (2015). https://doi.org/10.1021/acs.jpcc.5b10267
31. L. Zhang, B. Luan, R. Zhou, *J. Phys. Chem. B* **123**(34), 7243 (2019). https://doi.org/10.1021/acs.jpcb.9b02797
32. A. Govind Rajan, M.S. Strano, D. Blankschtein, *Nano Lett.* **19**(3), 1539 (2019). https://doi.org/10.1021/acs.nanolett.8b04335
33. A. Cardellini, F. Maria Bellussi, E. Rossi, L. Chiavarini, C. Becker, D. Cant, P. Asinari, M. Sebastiani, *Mater. Des.* **208**, 109902 (2021). https://doi.org/10.1016/j.matdes.2021.109902
34. H. Yaghoubi, M. Foroutan, *Phys. Chem. Chem. Phys.* **20**, 22308 (2018). https://doi.org/10.1039/C8CP03762K
35. H. Yaghoubi, M. Foroutan, *Appl. Surf. Sci.* **500**, 144002 (2020). https://doi.org/10.1016/j.apsusc.2019.144002
36. T. Koishi, K. Yasuoka, S. Fujikawa, X.C. Zeng, *ACS Nano* **5**(9), 6834 (2011). https://doi.org/10.1021/nn2005393
37. V. Sresht, A. Govind Rajan, E. Bordes, M.S. Strano, A.A.H. Pádua, D. Blankschtein, *J. Phys. Chem. C* **121**(16), 9022 (2017). https://doi.org/10.1021/acs.jpcc.7b00484
38. H. Liu, Y. Li, W.E. Krause, O.J. Rojas, M.A. Pasquinelli, *J. Phys. Chem. B* **116**(5), 1570 (2012). https://doi.org/10.1021/jp209024r
39. C. Zhu, Y. Gao, H. Li, S. Meng, L. Li, J.S. Francisco, X.C. Zeng, *Proc. Natl. Acad. Sci. U.S.A.* **113**(46), 12946 (2016). https://doi.org/10.1073/pnas.1616138113
40. S.A. Etha, P.R. Desai, H.S. Sachar, S. Das, *Macromolecules* **54**(2), 584 (2021). https://doi.org/10.1021/acs.macromol.0c02234
41. X.S. Wu, N. Wang, *J. Biomater. Sci. Polym. Ed.* **12**(1), 21 (2001). https://doi.org/10.1163/156856201744425
42. M. Parent, C. Nouvel, M. Koerber, A. Sapin, P. Maincent, A. Boudier, *J. Control. Release* **172**(1), 292 (2013). https://doi.org/10.1016/j.jconrel.2013.08.024
43. H.K. Makadia, S.J. Siegel, *Polymers* **3**(3), 1377 (2011). https://doi.org/10.3390/polym3031377

44. Chemical & Physical Properties of Select Polymers (n.d.). https://www.absor bables.com/technical/properties/

45. J. Andrews, R.A. Handler, E. Blaisten-Barojas, *Polymer* **206**, 122903 (2020). https://doi.org/10.1016/j.polymer.2020.122903

46. A. Khodayari, M. Fasano, M.B. Bigdeli, S. Mohammadnejad, E. Chiavazzo, P. Ansi-nari, *Case Stud. Therm. Eng.* **12**, 454 (2018). https://doi.org/10.1016/j.csite.2018.06.005

47. A. Pérez de la Luz, G.A. Méndez-Maldonado, E. Núñez-Rojas, F. Bresme, J. Alejandre, *J. Chem. Theory Comput.* **11**(6), 2792 (2015). https://doi.org/10.1021/acs.jctc.5b00080

48. C. Caleman, P.J. van Maaren, M. Hong, J.S. Hub, L.T. Costa, D. van der Spoel, *J. Chem. Theory Comput.* **8**(1), 61 (2012). https://doi.org/10.1021/ct200731v

49. R.A. Zubillaga, A. Labastida, B. Cruz, J.C. Martínez, E. Sánchez, J. Alejandre, *J. Chem. Theory Comput.* **9**(3), 1611 (2013). https://doi.org/10.1021/ct300976t

50. C. Vega, E. de Miguel, *J. Chem. Phys.* **126**(15), 154707 (2007). https://doi.org/10.1063/1.2715577

51. Dortmund Data Bank, Surface Tension of Hexane (n.d.). http://www.ddbst.com/en/EED/PCP/SFT_C89.php

52. Y.C. Jung, B. Bhushan, *Nanotechnology* **17**(19), 4970 (2006). https://doi.org/10.1088/0957-4484/17/19/033

53. T.T. Chau, W.J. Bruckard, P.T.L. Koh, A.V. Nguyen, *Adv. Colloid Interface Sci.* **150**(2), 106 (2009). https://doi.org/10.1016/J.CIS.2009.07.003

54. Z. Zhang, X. Wang, R. Zhu, Y. Wang, B. Li, Y. Ma, Y. Yin, *Polym. Sci. Ser. B* **58**, 720 (2016). https://doi.org/10.1134/S1560090416060191

55. W.F. van Gunsteren, X. Daura, N. Hansen, A.E. Mark, C. Oostenbrink, S. Riniker, L.J. Smith, *Angew. Chem. Int. Ed.* **57**(4), 884 (2018). https://doi.org/10.1002/anie.201702945

56. G. Hong-Kai, F. Hai-Ping, *Chin. Phys. Lett.* **22**(4), 787 (2005)

57. J. Zhang, M.K. Borg, K. Sefiane, J.M. Reese, *Phys. Rev. E* **92**(5), 052403 (2015)

58. M. Masuduzzaman, B. Kim, *Microfluid. Nanofluid.* **25**(6), 54 (2021)

59. M. Ricci, O.M. Roscioni, L. Querciagrossa, C. Zannoni, *Phys. Chem. Chem. Phys.* **21**, 26195 (2019). https://doi.org/10.1039/C9CP04120F

60. S. Prodhan, J. Qiu, M. Ricci, O.M. Roscioni, L. Wang, D. Beljonne, *J. Phys. Chem. Lett.* **11**(16), 6519 (2020). https://doi.org/10.1021/acs.jpclett.0c01793

61. F.M. Bellussi, O.M. Roscioni, M. Ricci, M. Fasano, *J. Phys. Chem. B* **125**(43), 12020 (2021). https://doi.org/10.1021/acs.jpcb.1c07642

62. H.G. Ozcelik, E. Satiroglu, M. Barisik, *Nanoscale* **12**(41), 21376 (2020). https://doi.org/10.1039/D0NR05392A

63. European Committee for Standardization: CEN Workshop Agreement CWA 17284: Materials modelling - Terminology, classification and metadata (2018). https://emmc.info/wp-content/uploads/2018/05/CWA_17284.pdf

64. European Committee for Standardization: CEN Workshop Agreement CWA 17815: Materials characterisation - Terminology, metadata and classification (2021). https://www.cencenelec.eu/media/CEN-CENELEC/CWAs/ICT/cwa17815.pdf

65. Y. Xu, D. Koo, E.A. Gerstein, C.-S. Kim, *Polymer* **84**, 121 (2016). https://doi.org/10.1016/j.polymer.2015.12.052

66. K. Pei, Y. Ying, C. Chu, *Mater. Today Chem.* **4**, 90 (2017). https://doi.org/10.1016/j.mtchem.2017.02.006

67. M. Pannuzzo, B.A.C. Horta, C. La Rosa, P. Decuzzi, *Macromolecules* **53**(10), 3643 (2020). https://doi.org/10.1021/acs.macromol.0c00110

68. J. Andrews, E. Blaisten-Barojas, *J. Phys. Chem. B* **123**(48), 10233 (2019). https://doi.org/10.1021/acs.jpcb.9b06681

69. M.D. Hanwell, D.E. Curtis, D.C. Lonie, T. Vandermeersch, E. Zurek, G.R. Hutchison, *J. Cheminform.* **4**(1), 17 (2012). https://doi.org/10.1186/1758-2946-4-17

70. Avogadro: An open-source molecular builder and visualization tool, version 1.XX (n.d.). http://avogadro.cc/

71. A.I. Jewett, D. Stelter, J. Lambert, S.M. Saladi, O.M. Roscioni, M. Ricci, L. Autin, M. Maritan, S.M. Bashusqeh, T. Keyes, R.T. Dame, J.-E. Shea, G.J. Jensen, D.S. Goodsell, *J. Mol. Biol.* **433**(11), 166841 (2021). https://doi.org/10.1016/j.jmb.2021.166841

72. S. Plimpton, *J. Comput. Phys.* **117**(1), 1 (1995). https://doi.org/10.1006/jcph.1995.1039

73. LAMMPS Molecular Dynamics Simulator (n.d.). https://www.lammps.org

74. S.W.I. Siu, K. Pluhackova, R.A. Böckmann, *J. Chem. Theory Comput.* **8**(4), 1459 (2012) https://doi.org/10.1021/ct200908r. https://doi.org/10.1021/ct200908r

75. J.L.F. Abascal, C. Vega, *J. Chem. Phys.* **123**(23), 234505 (2005). https://doi.org/10.1063/1.2121687

76. H.J.C. Berendsen, J.R. Grigera, T.P. Straatsma, *J. Phys. Chem.* **91**(24), 6269 (1987). https://doi.org/10.1021/j100308a038

77. I.-C. Yeh, M.L. Berkowitz, *J. Chem. Phys.* **111**(7), 3155 (1999). https://doi.org/10.1063/1.479595

78. Jmol: An open-source Java viewer for chemical structures in 3D (n.d.). http://www.jmol.org/

79. P. Cignoni, M. Callieri, M. Corsini, M. Dellepiane, F. Ganovelli, G. Ranzuglia, "MeshLab: An Open-Source Mesh Processing Tool," in P*roceedings of the Euro-graphics Italian Chapter Conference* (Eurographics Association, 2008), pp. 129. https://doi.org/10.2312/LocalChapterEvents/ItalChap/ItalianChapConf2008/129-136

80. D. Nečas, P. Klapetek, *Cent. Eur. J. Phys.* **10**, 181 (2012). https://doi.org/10.2478/s11534-011-0096-2

81. J.G. Kirkwood, F.P. Buff, *J. Chem. Phys.* **17**(3), 338 (1949). https://doi.org/10.1063/1.1747248

82. F.M. Bellussi, O.M. Roscioni, A. Cardellini, M. Provenzano, M. Fasano, *Zenodo* (2022). https://doi.org/10.5281/zenodo.6629427

83. P. Gentile, V. Chiono, I. Carmagnola, P.V. Hatton, *Int. J. Mol. Sci.* **15**(3), 3640 (2014). https://doi.org/10.3390/ijms15033640

84. D.L. Sedin, K.L. Rowlen, *Appl. Surf. Sci.* **182**(1), 40 (2001). https://doi.org/10.1016/S0169-4332(01)00432-9 □